

Specnuezhenide Alleviates Senile Osteoporosis by Activating TGR5/FXR Signaling in Bone Marrow Mesenchymal Stem Cells and RANKL-Induced Osteoclasts

Xuehui Deng^{1,2,*}, Bingfeng Lin^{1,*}, Wenlong Xiao³, Fang Wang², Pingcui Xu¹, Nani Wang¹⁻³

¹Department of Medicine, Zhejiang Academy of Traditional Chinese Medicine, Hangzhou, Zhejiang, People's Republic of China; ²School of Pharmacy, Zhejiang Chinese Medical University, Hangzhou, Zhejiang, People's Republic of China; ³School of Pharmacy, Hangzhou Medical College, Hangzhou, Zhejiang, People's Republic of China

*These authors contributed equally to this work

Correspondence: Nani Wang, Department of Medicine, Zhejiang Academy of Traditional Chinese Medicine, 132 Tianmushan Road, Hangzhou, Zhejiang, 310007, People's Republic of China, Tel/Fax +86-571-88849089, Email wnn8511@163.com

Background: Specnuezhenide (SPN) is an iridoid glycoside isolated from *Fructus Ligustri Lucidi*, an herb prescribed for the treatment of senile osteoporosis. However, the direct role of SPN on bone metabolism remains unclear. In this study, the effects of SPN on D-galactose (D-gal)-induced mice, bone marrow mesenchymal stem cells (BMSCs), and nuclear factor- κ B ligand-induced osteoclasts were examined.

Methods: Micro-computed tomography was used to observe the bone microstructure. Osteogenesis was examined using Western blotting and alkaline phosphatase staining. Osteoclastogenesis was examined using Western blotting and F-actin ring staining. Senescence-associated β -galactosidase was used to detect cell senescence. In addition, the expression of Takeda G protein-coupled receptor 5 (TGR5)/farnesoid X receptor (FXR) signaling pathway-related genes and proteins was determined through quantitative real-time polymerase chain reaction and immunofluorescence.

Results: Oral administration of SPN improved the bone microstructure in D-gal-induced mice and increased bone mineral density, bone volume, trabecular thickness, and trabecular number. SPN also upregulated the expression of the osteogenesis markers osteocalcin, bone morphogenetic protein 2, and runt-related transcription factor 2 and downregulated the expression of the osteoclast markers tartrate-resistant acid phosphatase, nuclear factor- κ B, and nuclear factor of activated T-cells in the D-gal-induced bone. Furthermore, SPN increased alkaline phosphatase staining, inhibited F-actin ring formation, and reduced the activity of senescence-associated β -galactosidase in vitro. Mechanistically, SPN activated the TGR5/FXR pathway in D-gal-induced BMSCs and osteoclasts. The protective effects of SPN were abolished after addition of the TGR5 inhibitor SBI-115 or FXR inhibitor DY268. Moreover, SPN could elevate the protein and mRNA levels of TGR5, FXR, and the downstream small heterodimer partner in D-gal-induced bone.

Conclusion: SPN alleviated senile osteoporosis and cell senescence by activating the TGR5/FXR pathway.

Keywords: specnuezhenide, Takeda G protein-coupled receptor 5, farnesoid X receptor, osteoporosis

Introduction

Senile osteoporosis is characterized by deterioration of the bone microstructure and reduced bone strength, resulting in a high fracture risk.¹ With the dramatic increase in the global population of older adults, this disease has emerged as a public health challenge worldwide.^{2,3} Bone loss can directly lead to bone fragility, and the cause of bone loss during aging is closely related to the aging of bone marrow mesenchymal stem cells (BMSCs).^{4,5} BMSCs have strong self-renewal ability and multidirectional differentiation potential, and can differentiate into a variety of cells, including osteoblasts.^{6,7} In addition to the osteogenic ability of osteoblasts, the normal growth of bone is also dependent on the

bone resorption of osteoclasts.⁸ Senescent-cell conditioned media have been shown to impair enhanced osteoclast-progenitor survival, leading to increased osteoclastogenesis.⁹ The expression of the bile acid receptors Takeda G protein-coupled receptor 5 (TGR5) and farnesoid X receptor (FXR) is downregulated in the aging bone. TGR5 knockdown has been shown to induce osteoclast differentiation to decrease bone mass in aged mice,¹⁰ while activation of FXR promotes the differentiation of BMSCs into osteoblasts.¹¹ FXR agonists have also been shown to suppress osteoclast differentiation from bone marrow macrophages.¹² A growing body of evidence has shown that TGR5 and FXR are important regulators in the development of senile osteoporosis. Thus, the TGR5/FXR signaling pathway is a promising target for mitigating senile osteoporosis.

Specnuezhenide (SPN) is an iridoid glycoside isolated from *Fructus Ligustri Lucidi*,¹³ which is clinically used in the treatment of senile osteoporosis.^{14,15} Administration of the extract of *Fructus Ligustri Lucidi* has been shown to restore bone mass in D-galactose (D-gal)-induced mice.¹⁶ SPN also shows anti-osteoporosis effects in streptozotocin-induced rats.¹⁷ However, the effects of SPN on senile osteoporosis have not been elucidated, and the role of SPN on BMSC and OC senescence remains especially unclear. In the present study, we examined the effects of SPN on the bone mass of D-gal-induced mice and the osteogenic activity of D-gal-induced BMSCs and OCs. Our results demonstrated that SPN improved bone microarchitecture, promoted bone formation, and suppressed bone resorption in vivo. SPN inhibited the senescence of cells in addition to increasing osteogenesis activity and decreasing osteoclastic activity in vitro. Mechanistically, SPN exerted osteoprotective effects, at least partly, by activating the TGR5/FXR pathway. Our study provided evidence to support the potential use of SPN as a preventive and therapeutic agent against senile osteoporosis.

Materials and Methods

Mice and Treatment

Male ICR mice (age, 8 weeks; weight, 20–22 g) were obtained from Hangzhou Medical College (Hangzhou, Zhejiang, China). All animal experiments were conducted in accordance with the NIH Guide for the Care and Use of Laboratory Animals (NIH Publication No. 80–23; revised 1978) and the Guidelines for Animal Experiments of the Zhejiang Academy of Traditional Chinese Medicine (Approval No. 2021–001). The protocol was approved by the Institutional Animal Ethics Committee. SPN (#102728; purity \geq 98%; Yongjian Pharmaceutical, Jiangsu, China; [Figure 1A](#)) was dissolved in sterile saline. The mice were randomly divided into the following groups: normal control group (CON: daily gastric irrigation [i.g.] of sterile saline + daily subcutaneous injection [s.q.] of sterile saline, n = 10), model group (MOD: daily i.g. of sterile saline + daily s.q. of 150 mg/kg/d D-gal, n = 10), low-dosage SPN (SPN-L: daily i.g. of 5 mg/kg/d SPN + daily s.q. of 150 mg/kg/d D-gal, n = 10), and high-dosage SPN (SPN-H: daily i.g. of 10 mg/kg/d SPN + daily s.q. of 150 mg/kg/d D-gal, n = 10). All treatments were performed for three months. The experimental diagram is shown in the text ([Figure 1B](#)). The number of animals per group was determined on the basis of previous reports.¹⁸ The dose and duration of SPN were also based on previous reports.^{19,20}

Micro-Computed Tomography Bone Analysis

Femurs were removed and kept in 4% formalin. Fixed femurs were scanned using a micro-computed tomography (micro-CT) scanner (Skyscan 1172; Bruker, Belgium). Values for bone mineral density (BMD), bone volume/total volume (BV/TV), trabecular thickness (Tb.Th), and trabecular number (Tb.N) were obtained.

Hematoxylin-Eosin Staining

Femurs were embedded in paraffin. Hematoxylin-eosin (HE) staining was performed using a standard protocol reported previously.¹³ The sections were stained with an HE assay kit (#G1076; Servicebio, Hubei, China).

Dynamic Histomorphometric Assessments of Bone Formation

The dynamic histomorphometry parameters measured included mineral apposition rate (MAR).²¹ The mice were injected with calcein (35 mg/kg, intraperitoneal injection [i.p.]; Sangon Biotech, Shanghai, China) and tetracycline (20 mg/kg, i. p.; Aladdin, Shanghai, China) dissolved in sterile saline at 10 and 2 days before harvesting the femurs. The femurs were

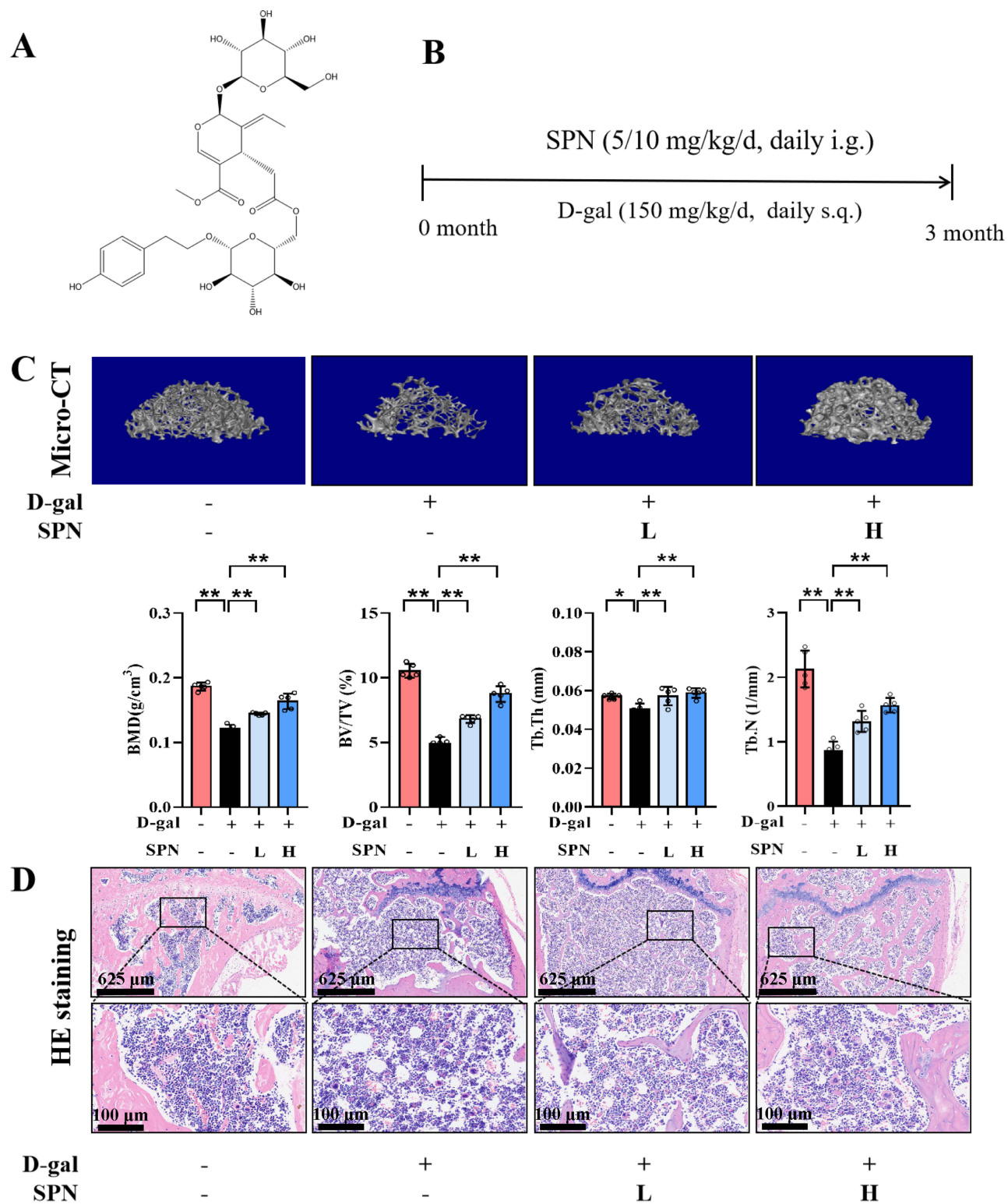


Figure 1 SPN improved bone microarchitecture in D-gal-induced mice. **(A)** SPN structure. **(B)** Experimental diagram. **(C)** Micro-CT images of trabecular bone at the femur and trabecular microarchitecture parameters (n=5). **(D)** HE staining image of femur (n=5). Data are expressed as the mean ± SD. *P < 0.05, **P < 0.01 compared with the MOD group.

embedded in methyl methacrylate (#M813511; Macklin, Shanghai, China) to form blocks, and sectioned into 10- μ m slices. The sections were viewed under a fluorescent Panoramic MIDI system (3DHISTECH).

Western Blotting Analysis

The tibia was homogenized and extracted in RIPA lysis buffer (Beyotime, Shanghai, China). The protein content was measured using a BCA kit (Keygentec, Nanjing, China). The primary antibodies included anti-FXR (#DF12402; Affinity, Jiangsu, China), anti-TGR5 (#DF14087; Affinity), anti-small heterodimer partner (SHP, #AF6244; Affinity), anti-alkaline phosphatase (ALP, #BM4284; Boster, Hubei, China), anti-runt-related transcription factor 2 (Runx2, #DF0171; Boster), anti-bone morphogenetic protein 2 (BMP2, #AF5163; Affinity), anti-nuclear factor- κ B (RANK, #DF12532; Affinity), and anti-nuclear factor of activated T-cells (NFATc1, #D0522; Santa Cruz Biotechnology). The membrane was incubated with goat anti-rabbit IgG. Protein band densities were analyzed using ImageJ software and normalized to the GAPDH level.

Immunohistochemistry

Femurs were collected, fixed with 4% formalin for 48 h, decalcified in 10% ethylenediaminetetraacetic acid (EDTA), paraffin-embedded, and used for tartrate-resistant acid phosphatase (TRAP) and Masson's trichrome staining.^{22,23} Next, 5- μ m sections were incubated with primary antibodies against osteocalcin (OCN, #DF12303; Boster), TGR5, FXR, P16 (#AF0228, Affinity), P21 (#DF6423, Affinity), P53 (#AF0879, Affinity), and CD146 (#17564-1-AP, Proteintech). The images were analyzed by Image-Pro Plus 6.0 software (Media Cybernetics, Silver Spring, USA).

Cell Culture and Treatment

BMSCs and RAW264.7 cells were purchased from the National Collection of Authenticated Cell Cultures (Shanghai, China). Cells were cultured in Dulbecco's modified essential medium supplemented with 10% fetal bovine serum and 1% antibiotics, and cultured at 37°C in a humidified atmosphere containing 5% CO₂ until confluence. To generate osteoclasts, RAW264.7 cells (3×10^3 cells/well) were cultured in the presence of 50 ng/mL nuclear factor- κ B ligand (RANKL) and various additives. BMSCs and OC were respectively divided into the following groups: blank control group, D-gal group (D-gal, 50 mM), D-gal + SPN group (D-gal, 50 mM; SPN, 10^{-1} μ M), D-gal + SPN + SBI-115 group (D-gal, 50 mM; SPN, 10^{-1} μ M; SBI-115, 1 μ M), D-gal + SPN + DY268 group (D-gal, 50 mM; SPN, 10^{-1} μ M; DY268, 1 μ M), and D-gal + SPN + SBI-115 + DY268 group (D-gal, 50 mM; SPN, 10^{-1} μ M; SBI-115, 1 μ M; DY268, 1 μ M). After treatment for 48 h, the cells were collected for senescence-associated β -galactosidase (SA- β -gal) staining.

SA- β -gal Staining

SA- β -gal staining was performed in accordance with the manufacturer's instructions (#C0602, Beyotime). Briefly, cells were fixed in 4% paraformaldehyde for 15 min and incubated with SA- β -gal staining solution at 37°C for 12 h. The cells were washed with phosphate-buffered saline (PBS) and photographed under a microscope (TI-DH; Nikon, Tokyo, Japan). The percentage of SA- β -gal-positive cells was expressed as the ratio of blue-stained cells to the total number of cells.

ALP Staining

After the BMSCs reached 80% confluence, the medium was replaced with an osteogenic induction medium (100 nM dexamethasone, 10 mM β -glycerophosphate, and 50 μ M ascorbic acid). D-gal, SPN, SBI-115, and DY268 were added to the osteogenic induction medium in accordance with the experimental design. After culturing for 7 days, ALP staining measurements were conducted. For ALP staining, cells were washed with PBS three times and stained using an ALP staining kit (#C3206, Beyotime).^{24,25} The cells were washed with water and photographed under a microscope.

F-Actin Ring Staining

After 5 d of OC induction, the cells were fixed with 4% paraformaldehyde, permeabilized with 0.1% Triton X-100 in PBS for 5 min, and then stained with fluorescein isothiocyanate (FITC)-phalloidin solution (#C1033, Beyotime) in darkness for 1 h. After washing with PBS, the cells were incubated with a 4',6-diamidino-2-phenylindole (DAPI) solution

for 10 min to stain the nuclei. The images of F-actin rings were visualized under a confocal microscope (LSM800; Zeiss, Oberkochen, Germany).

RNA Sequencing

RNA was isolated using TRIzol reagent. Sequencing libraries were generated using the ALFA-SEQ Directional RNALib Prep Kit (mChip, Guangzhou, China). The mRNA was purified using poly-T oligo-attached magnetic beads. First-strand cDNA was prepared using random hexamer primers and M-MuLV reverse transcriptase (RNase H). Second-strand cDNA was synthesized using DNA polymerase I and RNase H. Library quality was assessed on a Qsep400 high-throughput nucleic acid protein analysis system (Houze Biotechnology Co., Ltd., Hangzhou, China). Genes were considered to be differentially expressed when the fold changes were ≥ 2 and the corrected P value was < 0.05 .

Immunofluorescence Staining

Cells were fixed with 4% paraformaldehyde for 15 min and permeabilized with 0.1% Triton X-100 (this step was omitted for TGR5). Cells were incubated with anti-TGR5 (dilution 1:500) or anti-FXR (dilution 1:500) antibodies at 4°C for 12 h, and then incubated with goat pAb to Rb IgG (Alexa Fluor® 488, #ab150077, Abcam) at room temperature for 1 h. The slides were mounted with DAPI and photographed under a confocal microscope.

RNA Isolation and Real-Time Reverse Transcription Polymerase Chain Reaction

Total RNA was extracted from tibias using TRIzol (Invitrogen, Carlsbad, CA, US). The RNA sample was reverse-transcribed using a TOBOBlue qRT Premix with a gDNA Eraser 2.0 kit (#RTQ202, Toroid Technology, Shanghai, China). The mRNA expression levels of SHP, TGR5, and FXR were measured in a 7500 quantitative real-time reverse transcription polymerase chain reaction system (RT-PCR; Applied Biosystems, Waltham, MA, US) using SYBR Green reagents (#QPS201; Toyobo, Osaka, Japan). The primer sequences are listed in [Table S1](#). Relative mRNA expression was quantified by comparing cycle threshold values. GAPDH was used as a housekeeping gene, and data were presented as the fold change relative to the control.

Statistical Analysis

Statistical analysis was performed using GraphPad Prism 9.0 (GraphPad, CA, US). Data were presented as the mean \pm standard deviation. Statistical comparisons were performed using one-way or two-way analysis of variance followed by Dunnett corrections to compare multiple groups. $P < 0.05$ was considered statistically significant.

Results

SPN Promotes Osteoporosis in d-gal-Induced Mice

To determine the effect of SPN on bone microstructure, micro-CT analysis was performed on mouse femurs. The SPN-L and SPN-H groups showed higher BMD ([Figure 1C](#), $P < 0.01$), BV/TV ($P < 0.01$), Tb.N ($P < 0.01$), and Tb.Th ($P < 0.01$) in comparison with the corresponding values in the MOD group. HE staining showed that the cancellous bone in the femur in the D-gal group was significantly lower than that in the control group, and the trabecular bone arrangement was sparse, while the amount of cancellous bone increased and the thickness of trabecular bone widened after SPN administration ([Figure 1D](#)). These findings suggested that SPN improved osteoporosis in D-gal-induced mice.

SPN Increases Bone Formation in d-gal-Induced Mice

OCN is specifically secreted by osteoblasts and is considered an essential biomarker of bone formation.²⁶ The expression of OCN was downregulated in the MOD group in comparison with that in the CON group ([Figure 2A](#), $P < 0.01$), while SPN restored OCN expression ($P < 0.01$). SPN also promoted the expression of ALP ([Figure 2B](#), $P < 0.05$ for SPN-L and $P < 0.01$ for SPN-H), BMP2 ($P < 0.01$ for SPN-H), and Runx2 ($P < 0.01$) in D-gal-induced tibias in comparison with the corresponding expression levels in the MOD group. MAR expression was significantly lower in MOD mice in comparison with CON mice ([Figure S1A](#), $P < 0.01$), but SPN reduced this suppression ($P < 0.01$). Masson's trichrome

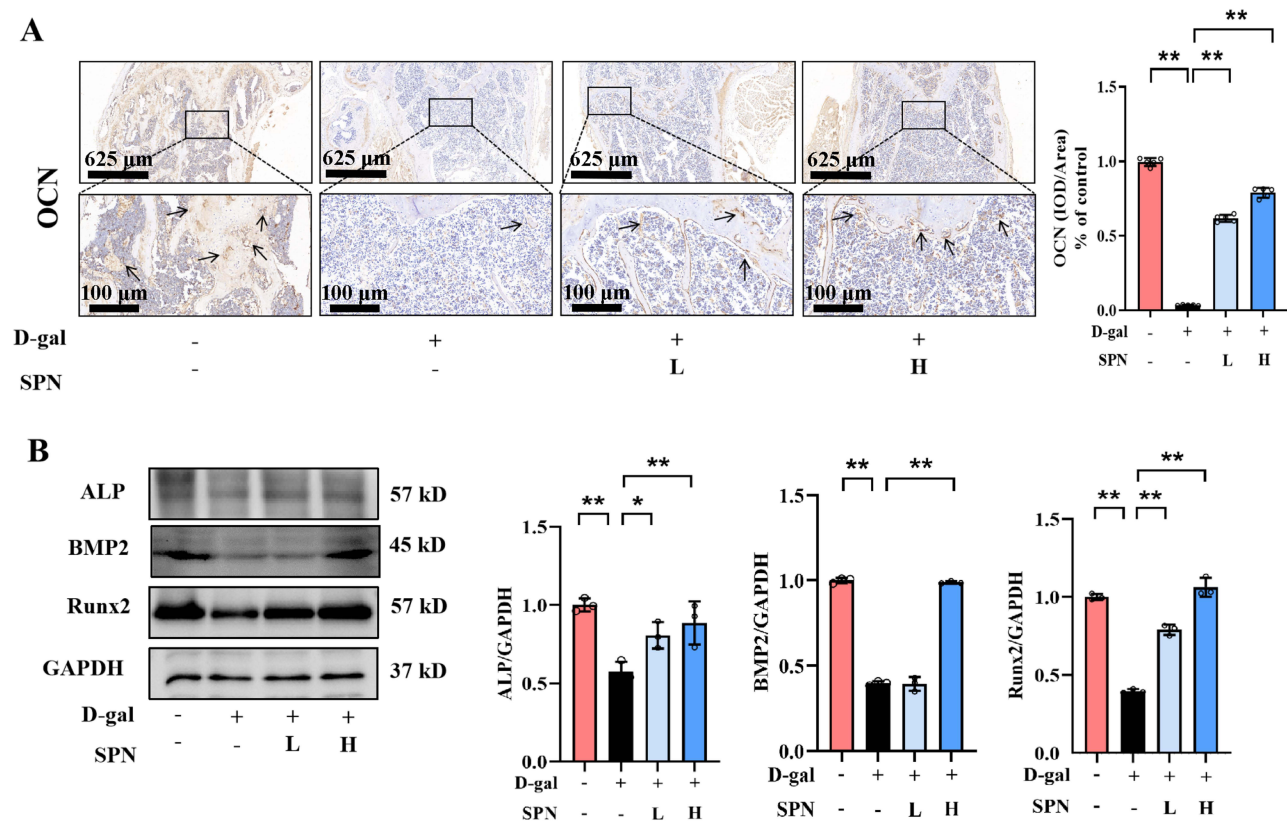


Figure 2 SPN improved bone formation in D-gal-induced mice. **(A)** IHC analysis of OCN in the femur (black arrows, $n=5$). **(B)** Western blotting analysis of ALP, BMP2 and Runx2 in tibias ($n=3$). Data are expressed as the mean \pm SD. * $P < 0.05$, ** $P < 0.01$ compared with the MOD group.

staining showed that SPN increased the number of osteoblasts in D-gal-induced mice (Figure S1B, $P < 0.01$). These results showed that SPN could promote bone formation in D-gal-induced mice.

SPN Decreases Bone Resorption in d-gal-Induced Mice

TRAP staining was performed to examine whether SPN alleviated D-gal-induced bone resorption. The number of osteoclasts in the femur in the MOD group was higher than that in the CON group (Figure 3A and B, $P < 0.01$), but the osteoclast number was reduced by SPN ($P < 0.01$). These results indicated that SPN suppressed bone resorption in D-gal-induced mice. The protein expression of RANK and NFATc1 was upregulated in the MOD group in comparison with the findings in the CON group (Figure 3C, $P < 0.01$), while SPN reversed these changes ($P < 0.01$).

SPN Attenuates Bone Senescence in d-gal-Induced Mice

Cellular senescence is a master issue in the development of age-related osteoporosis, so we measured the effect of SPN on senescence markers in mouse femurs. The expression levels of the senescence-related proteins P16, P21, and P53 were significantly higher in model mice (Figure 4A and B, $P < 0.01$) in comparison with those in the control group. SPN downregulated the expression levels of these proteins in comparison with those in the model group in a dose-dependent manner ($P < 0.01$).

SPN Attenuates Cell Senescence Through the TGR5/FXR Pathway

To study the effects of SPN on BMSCs and RAW264.7 cells, we detected the proliferation rates of the two kinds of cells under different concentrations of SPN, and found that the proliferation rates of the two kinds of cells under different concentrations of SPN did not differ from those in the control group (Figure S2A and B), suggesting that SPN was not toxic to cells. We also detected SA- β -gal-positive cells to evaluate the anti-senescence effects of SPN. As expected, D-gal

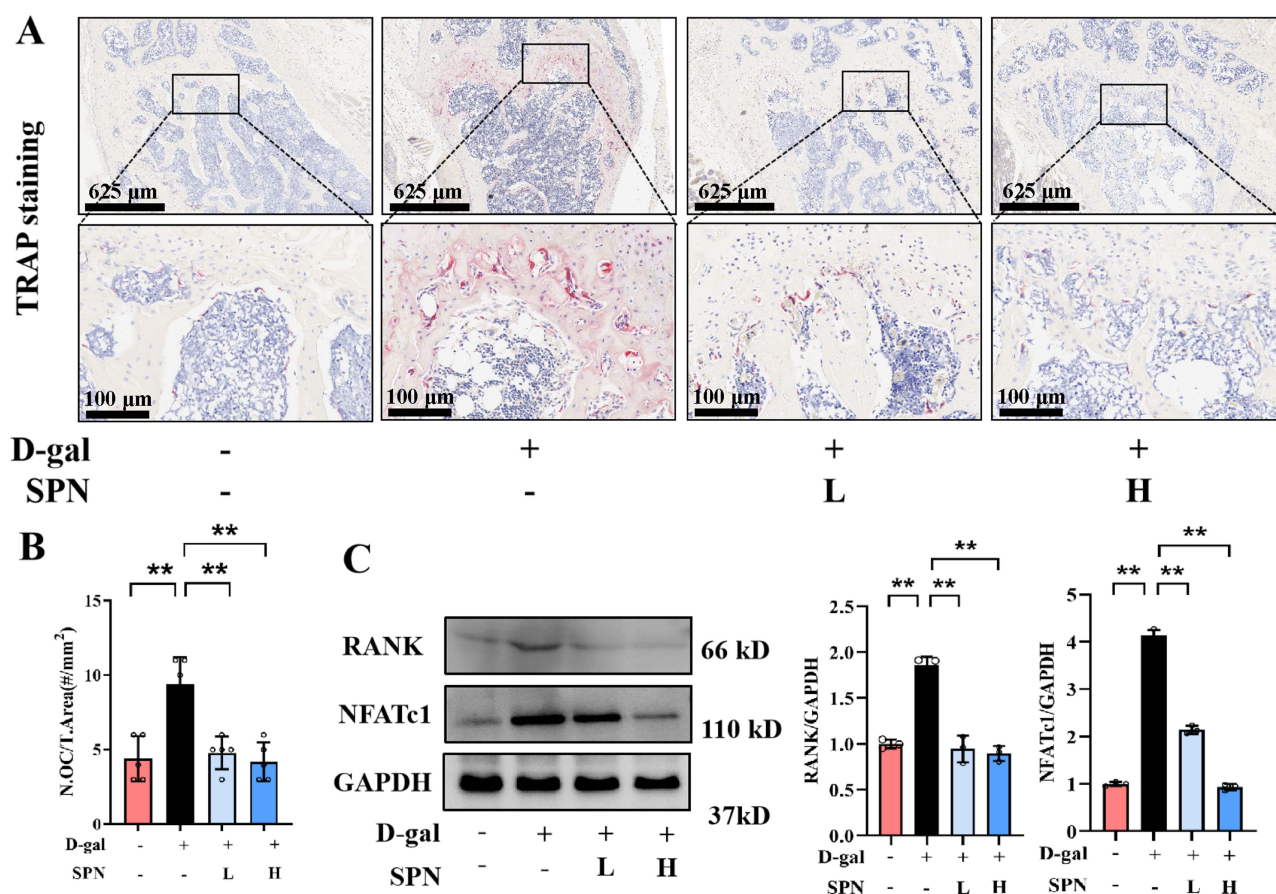


Figure 3 SPN suppressed bone resorption in D-gal-induced mice. **(A)** Representative TRAP-stained histological sections of femurs from D-gal-induced mice. **(B)** The number of osteoclasts/The area of tissue (N.Oc/T.Area) was analyzed. **(C)** Western blotting analysis of RANK and NFATc1 in tibias (n=3). Data are expressed as the mean \pm SD. ** $P < 0.01$ compared with the MOD group.

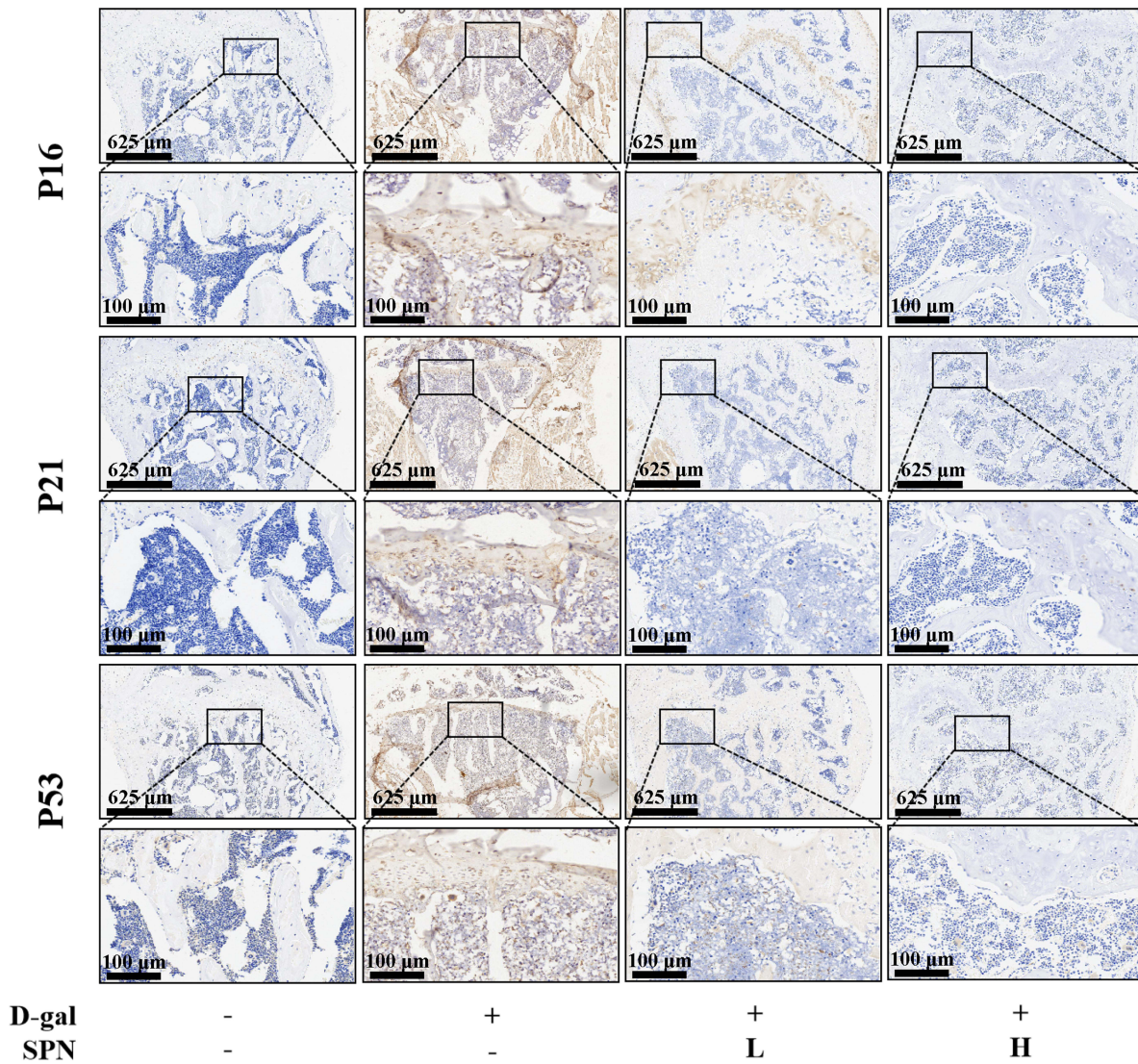
treatment increased the ratio of SA- β -gal-positive cells (Figure 5, $P < 0.01$). However, the corresponding ratio in the SPN group was lower than that in the MOD group ($P < 0.01$). Additionally, the combination of SBI-115 and DY268 increased the number of senescent cells in comparison with that in the D-gal + SPN + SBI-115 group ($P < 0.01$) or the D-gal + SPN + DY268 group ($P < 0.01$).

SPN Promoted Osteogenic Differentiation of BMSCs and Blocked Osteoclast Differentiation of RAW264.7 Cells Through the TGR5/FXR Pathway

BMSCs are identified by detection of CD146, a mesenchymal stem cell marker (Figure S3).²⁷ ALP is an early-stage osteogenic-differentiation marker.²⁸ The osteogenic induction medium induced osteogenic differentiation of BMSCs along with upregulation of ALP expression. SPN also increased the expression of ALP (Figure 6A). To confirm whether activation of TGR5 and FXR can induce ALP generation in BMSCs, we detected the ALP level in BMSCs after stimulation with the TGR5 antagonist SBI-115 or FXR antagonist DY268. SBI-115 and DY268 suppressed ALP expression. As a result, the osteogenic-differentiation effect of SPN was blocked in the presence of the SBI-115 or DY268.

Formation of F-actin-rich adhesive structures by osteoclasts is an essential step in bone resorption.²⁹ RANKL stimulation increased well-defined F-actin sealing rings with greater ring heights. The F-actin rings in the MOD group showed a typically huge ring structure (Figure 6B), those in the SPN group were obviously smaller. RANKL-induced RAW264.7 cells were also abrogated by the TGR5 antagonist SBI-115 or FXR antagonist DY268. The TRAP results showed that in comparison with the control group, the number and area of OCs in the model group were higher, while SPN administration alleviated this phenomenon (Figure S4). These results indicate that SPN can inhibit OC differentiation.

A



B

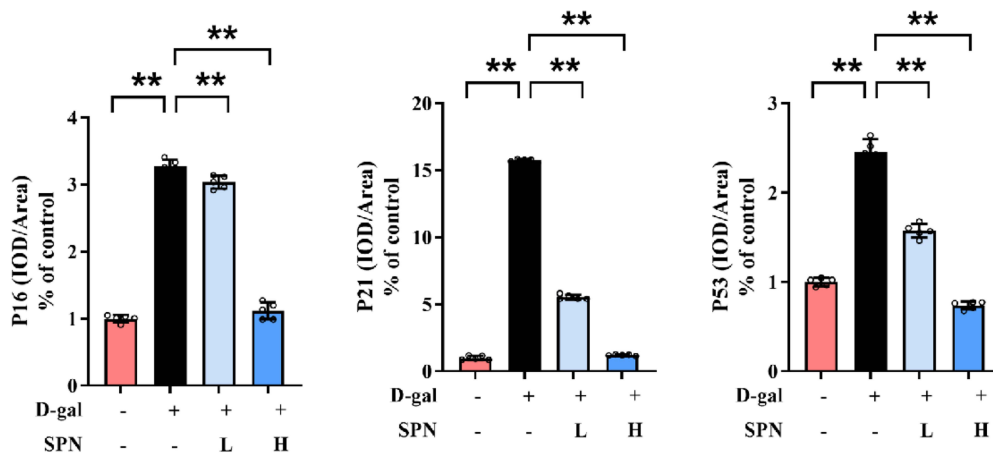


Figure 4 SPN attenuated senescence in D-gal-induced mice. **(A)** Immunohistochemistry of P16, P21, P53 and **(B)** related statistical analysis (n=5). Data are expressed as the mean ± SD. **P < 0.01 compared with the MOD group.

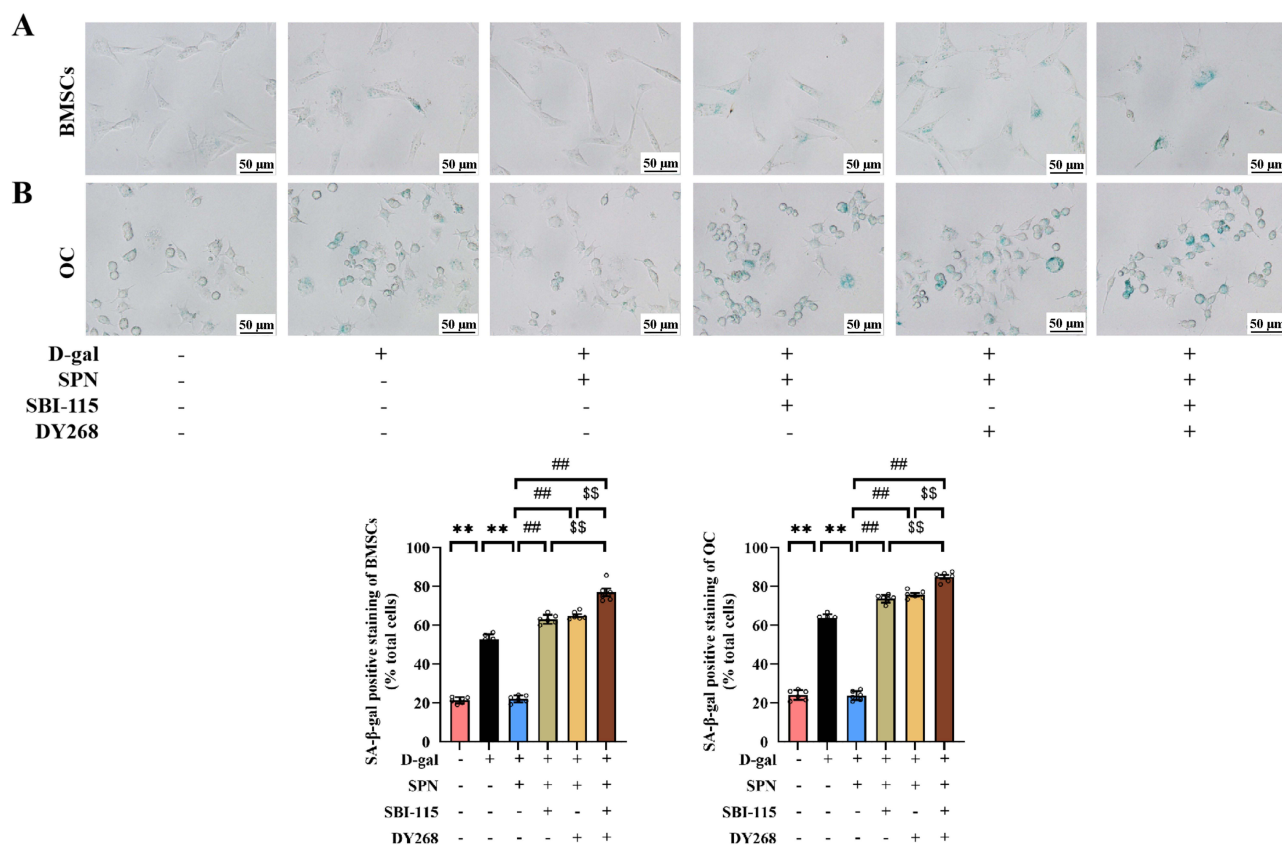


Figure 5 SPN inhibited the SA-β-gal-stained positive cells. **(A)** SA-β-gal staining of BMSCs. **(B)** SA-β-gal staining of OC. ** $P < 0.01$ compared with D-gal group. ## $P < 0.01$ compared with D-gal + SPN group. \$\$ $P < 0.01$ compared with D-gal + SPN + SBI-115 + DY268 group.

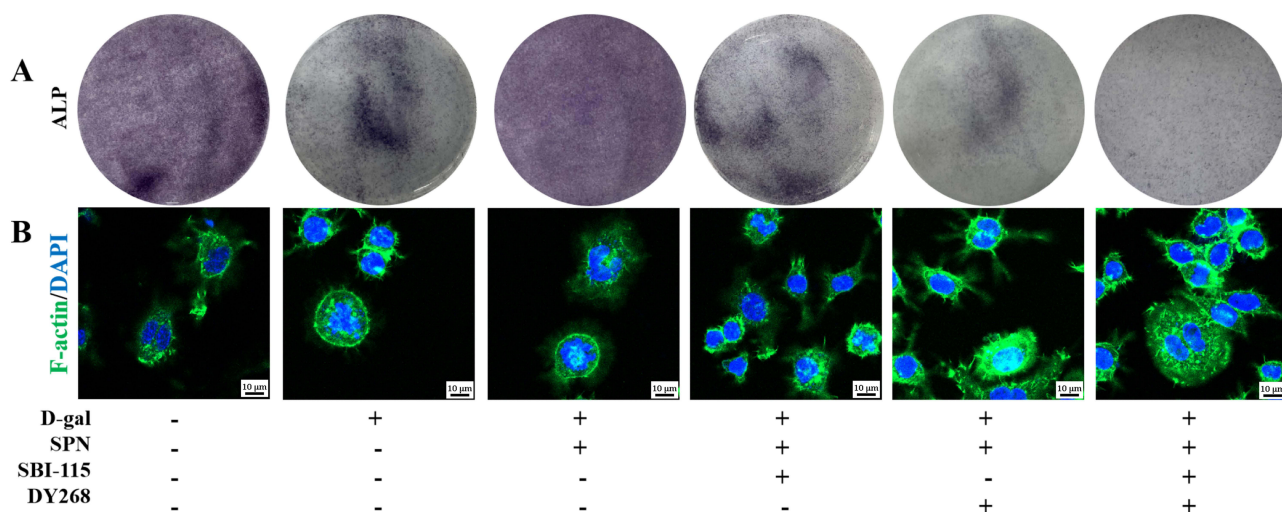


Figure 6 SPN promoted of ALP expression and inhibited of F-actin formation. **(A)** ALP staining. **(B)** F-actin staining.

SPN Upregulates TGR5 and FXR Expression in d-gal-Induced BMSCs and OCs

Next, we performed BMSC RNA-sequence analysis to explore the molecular mechanisms underlying the effects of SPN. In comparison with the expression levels in the model group, FXR predominated the upregulated genes (Figure 7A). Gene set enrichment analysis (GSEA) also revealed that SPN could regulate bile acid biosynthetic process-related genes (Figure 7B and C). To confirm whether SPN functions through TGR5-FXR activation, we evaluated TGR5 and FXR

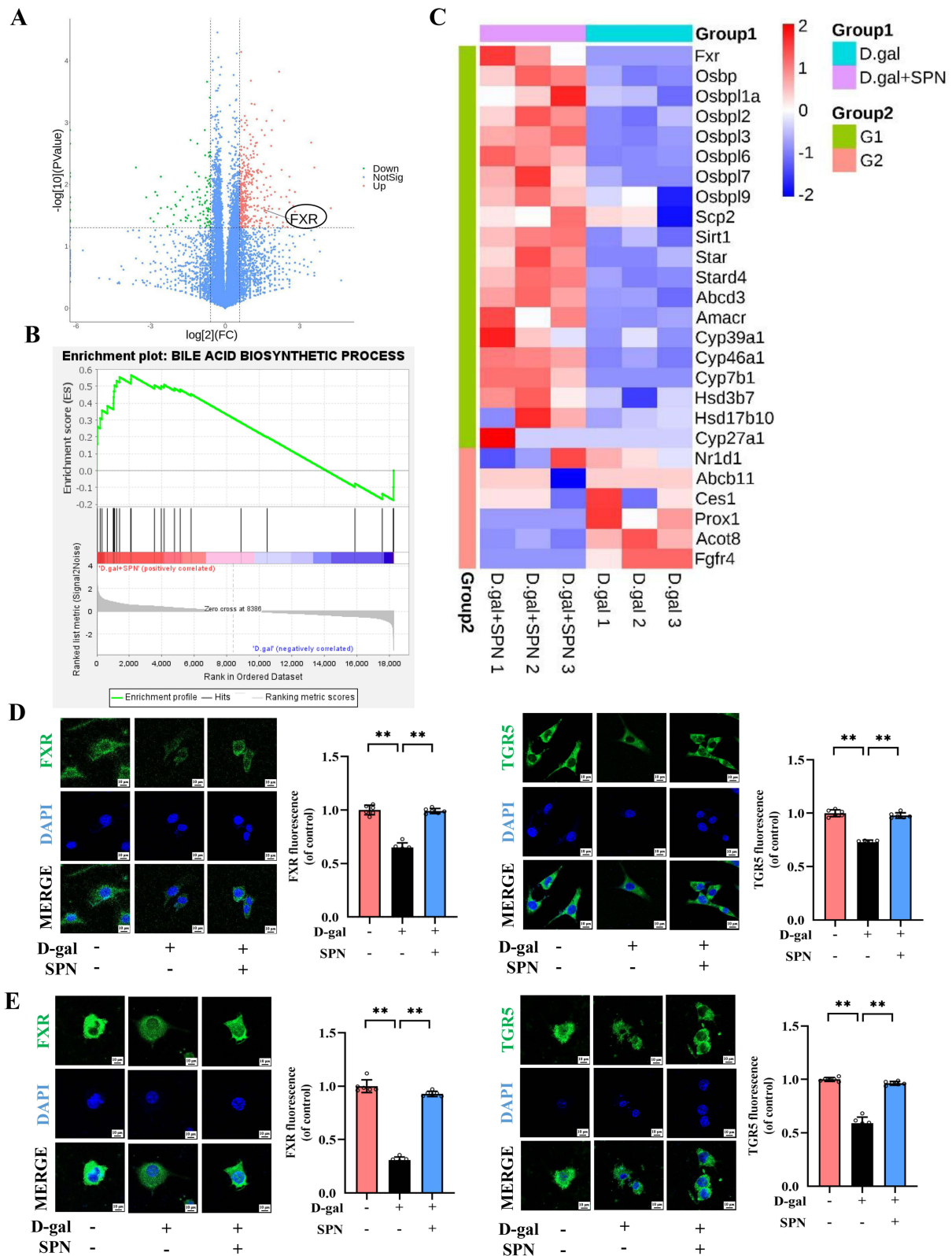


Figure 7 SPN increased TGR5 and FXR expression in D-gal-induced BMSCs and OC. **(A)** Changed genes in D-gal + SPN group compared with D-gal group displayed in volcano plot assay. **(B)** GSEA showing the bile acid biosynthetic process in D-gal + SPN group compared with D-gal group. **(C)** Changed bile acid biosynthetic process-related genes in D-gal + SPN group compared with D-gal group displayed in heatmap assay. Immunofluorescence analysis of TGR5 and FXR in **(D)** BMSCs and **(E)** OC (n=6). Scale bar, 10 μ m. Data are expressed as the mean \pm SD. ***P* < 0.01 compared with D-gal group.

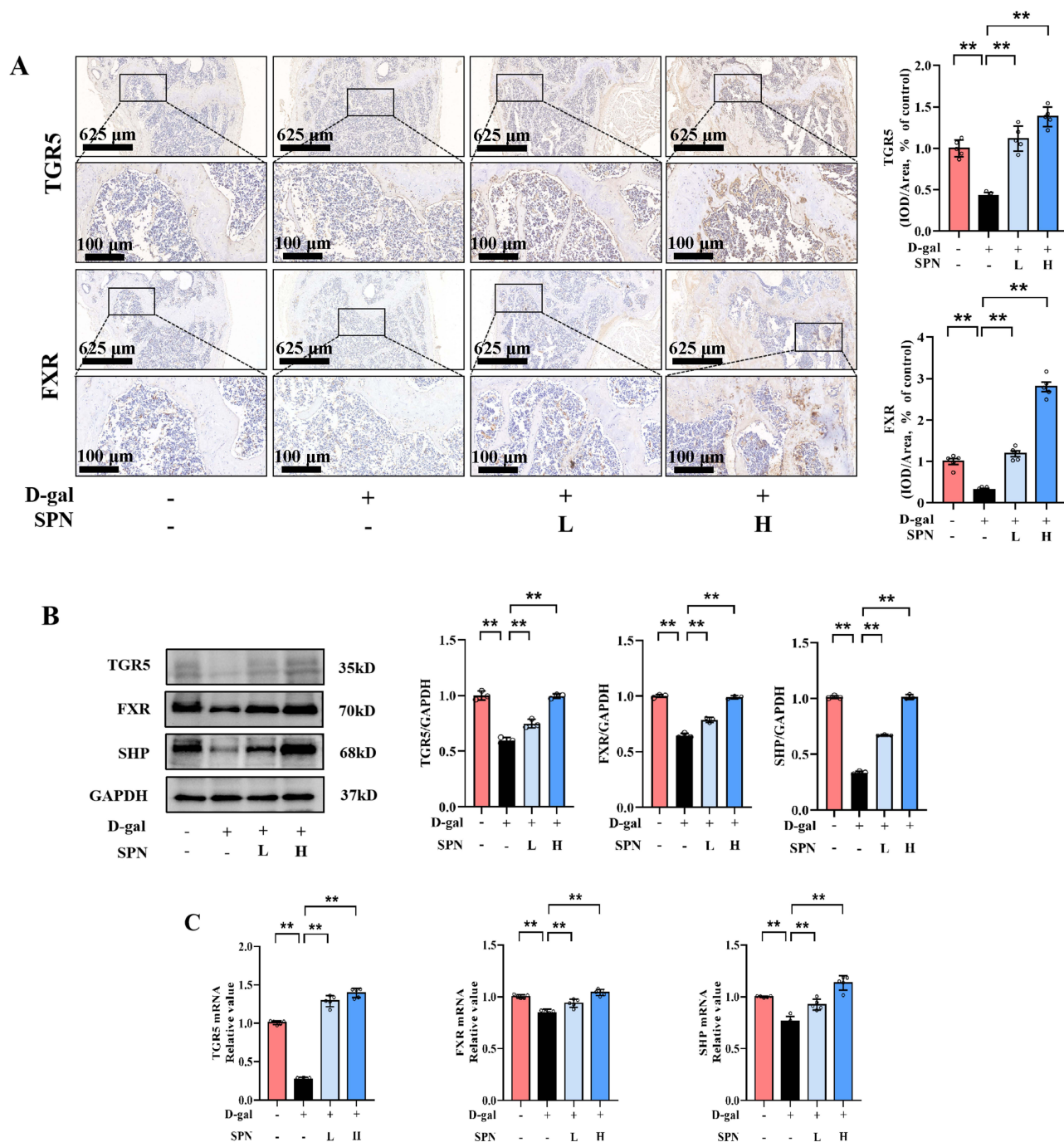


Figure 8 SPN enhanced TGR5 and FXR expression in the D-gal-induced mice. **(A)** IHC analysis of TGR5 and FXR in femurs (black arrows, $n=5$). **(B)** Western blotting analysis of TGR5, FXR, and SHP in tibias ($n=3$). **(C)** TGR5, FXR and SHP mRNA in tibias ($n=5$). Data are expressed as the mean \pm SD. $**P < 0.01$ compared with the MOD group.

expression in vitro (Figure 7D and E). D-gal exposure decreased the levels of TGR5 ($P < 0.01$) and FXR ($P < 0.01$), but SPN significantly elevated TGR5 ($P < 0.01$) and FXR ($P < 0.01$) expression in D-gal-induced BMSCs and OC.

SPN Activates TGR5 and FXR in d-gal-Induced Mice

We next examined the effects of SPN on TGR5 and FXR expression in bone tissues. The protein levels of TGR5 (Figure 8A, $P < 0.01$) and FXR ($P < 0.01$) were downregulated in the MOD group in comparison with the CON group, while SPN increased TGR5 and FXR expression ($P < 0.01$). Western blot results showed that SPN significantly

upregulated the protein expression levels of TGR5 (Figure 8B, $P < 0.01$), FXR ($P < 0.01$), and its downstream SHP ($P < 0.01$) in mouse tibias in comparison with those in the MOD group.

SPN treatment also upregulated the mRNA expression of TGR5 (Figure 8C, $P < 0.01$), FXR ($P < 0.01$), and SHP ($P < 0.01$) in D-gal-induced tibias. These data demonstrate that SPN treatment stimulated the TGR5-FXR pathway in D-gal-induced bone.

Discussion

A variety of active ingredients have been identified in *Fructus Ligustri Lucidi*. Previous investigations by our group and other researchers have shown that the aqueous extract and some compounds of *Fructus Ligustri Lucidi* are beneficial for bone metabolism.³⁰ However, the direct osteoprotective effects of SPN, the major active component of *Fructus Ligustri Lucidi*, in aging models remain to be elucidated. The present study is the first to demonstrate that administration of SPN increased the bone mass of D-gal-induced mice and attenuated cell senescence. The mechanism underlying this anti-osteoporosis effect may be linked to the improvement of bone formation and inhibition of bone resorption through promotion of osteoblastic differentiation of BMSCs and suppression of osteoclastic differentiation of RAW264.7 cells via activation of the TGR5/FXR pathway.

D-Gal is used to establish senile osteoporosis models.³¹ Exposure of mice to D-gal triggers the acceleration of natural senescence, which results in the induction of senile osteoporosis.³² Cell senescence and impaired osteogenic differentiation have also been observed in D-gal-induced BMSCs.³³ In this study, D-gal injection significantly decreased bone mass in mice. We also observed that the senescent-cell ratio was increased in D-gal-exposed BMSCs and OCs. Importantly, SPN effectively improved bone microarchitecture and increased the levels of osteogenesis markers, such as ALP, OCN, BMP2, and Runx2. Furthermore, the activities of SPN regulated osteoclast differentiation by downregulating the expression of TRAP, RANK, and NFATc1 and inhibiting F-actin formation. Altogether, these results suggest that SPN can stimulate the osteoblastic differentiation of BMSCs, suppress osteoclast differentiation of RAW264.7 cells, and attenuate senile osteoporosis.

TGR5 and FXR are bile acid receptors that serve as essential regulators in the development of senile osteoporosis.^{34,35} TGR5 deletion has been shown to markedly decrease bone mass in aged and ovariectomized mice.⁶ Upregulation of TGR5 can promote osteoblast mineralization and increase the expression of osteoblast differentiation marker genes.³¹ TGR5 regulates osteoclast differentiation to reduce bone loss.³⁶ FXR has also been shown to suppress osteoclast differentiation and promote osteoblast differentiation.¹¹ FXR typically heterodimerizes with the retinoid X receptor in FXR response elements associated with the promoters of the target gene Runx2, which is a bone-specific transcription factor. Deletion of FXR in vivo leads to significant bone loss.³⁷ In this study, we observed that SPN increased the levels of TGR5 and FXR and the bone formation biomarkers Runx2, OCN, BMP2, and ALP in D-gal-induced mice. In addition, SPN suppressed the expression of the bone resorption biomarkers TRAP, RANK, NFATc1, and F-actin. SPN may play bone-protective roles by activating the TGR5/FXR pathway in D-gal-induced bone. These results agreed with the findings of previous studies that demonstrated the beneficial effects of TGR5 and FXR on bone protection. The present study also confirmed the role of the TGR5/FXR pathway in the effects of SPN on D-gal-induced BMSCs and OCs by using a TGR5 antagonist (SBI-115) and an FXR antagonist (DY268). These findings indicated that SPN effectively promoted osteoblastic differentiation of BMSCs, inhibited osteoclastic differentiation of RAW264.7 cells, and alleviated cell senescence by activating the TGR5/FXR pathway.

Conclusions

In summary, this study is the first to demonstrate that SPN alleviates senile osteoporosis. This effect was associated with activation of the TGR5/FXR pathway, stimulation of osteoblastic differentiation of BMSCs, inhibition of osteoclastic differentiation of RANKL-induced RAW264.7 cells, and attenuation of cell senescence. Future studies should further evaluate the toxicity of this compound and investigate its anti-osteoporosis effects in females. These findings provide a theoretical basis for the use of SPN as a functional supplement in preventing and treating osteoporosis.

Abbreviations

Alkaline phosphatase (ALP), bone mesenchymal stem cells (BMSCs), bone mineral density (BMD), bone morphogenetic protein 2 (BMP2), bone volume/total volume (BV/TV), D-galactose (D-gal), ethylenediamine tetraacetic acid (EDTA), farnesoid X receptor (FXR), gene set enrichment analysis (GSEA), gastric irrigation (ig), immunohistochemistry (IHC), micro-computed tomography (micro-CT), osteoclast (OC), osteocalcin (OCN), nuclear factor- κ B ligand (RANKL), nuclear factor- κ B (RANK), nuclear factor of activated T-cells (NFATc1), real-time reverse transcription polymerase chain reaction (RT-PCR), runt-related transcription factor 2 (Runx2), subcutaneous injection (sq), senescence-associated β -galactosidase (SA- β -gal), small heterodimer partner (SHP), specnuezhenide (SPN), Takeda G protein receptor 5 (TGR5), trabecular number (Tb.N), trabecular thickness (Tb.Th), Tartrate-resistant acid phosphatase (TRAP).

Funding

This work was supported by National Natural Science Foundation of China (82374012), Zhejiang Provincial Natural Science Foundation of China (LHDMZ25H280004), Zhejiang Provincial Medicine Foundation (2022ZX002, 2021ZYY28, GZY-ZJ-KJ-23006, 2024ZR001), and Zhejiang Province Chai Xiujian Famous old TCM expert inheritance studio construction project.

Disclosure

The authors report no conflicts of interest in this work.

References

- Qadir A, Liang S, Wu Z, et al. Senile osteoporosis: the involvement of differentiation and senescence of bone marrow stromal cells. *Int J mol Sci.* 2020;21:349. doi:10.3390/ijms21010349
- Guo Y, Jia X, Cui Y, et al. Sirt3-mediated mitophagy regulates AGEs-induced BMSCs senescence and senile osteoporosis. *Redox Biol.* 2021;41:101915. doi:10.1016/j.redox.2021.101915
- Jiang YY, Li JD, Xue X, et al. Engineered extracellular vesicles for bone therapy. *Nano Today.* 2022;44:101487. doi:10.1016/j.nantod.2022.101487
- Hu M, Xing L, Zhang L, et al. NAP1L2 drives mesenchymal stem cell senescence and suppresses osteogenic differentiation. *Aging Cell.* 2022;21:e13551. doi:10.1111/ace1.13551
- Guo J, Wang F, Hu Y, et al. Exosome-based bone-targeting drug delivery alleviates impaired osteoblastic bone formation and bone loss in inflammatory bowel diseases. *Cell Rep Med.* 2023;4:100881. doi:10.1016/j.xcrm.2022.100881
- Zeng ZL, Xie H. Mesenchymal stem cell-derived extracellular vesicles: a possible therapeutic strategy for orthopaedic diseases: a narrative review. *Biomater Transl.* 2022;3:175–187. doi:10.12336/biomatertransl.2022.03.002
- Deng S, Zhu F, Dai K, et al. Harvest of functional mesenchymal stem cells derived from in vivo osteo-organoids. *Biomater Transl.* 2023;4:270–279. doi:10.12336/biomatertransl.2023.04.006
- Wang J, Li X, Wang S, et al. Bone-targeted exosomes: strategies and applications. *Adv Healthc Mater.* 2023;12:e2203361. doi:10.1002/adhm.202203361
- Farr JN, Xu M, Weivoda MM, et al. Targeting cellular senescence prevents age-related bone loss in mice. *Nat Med.* 2017;23:1072–1079. doi:10.1038/nm.4385
- Li L, Chen B, Zhu R, et al. *Fructus Ligustri Lucidi* preserves bone quality through the regulation of gut microbiota diversity, oxidative stress, TMAO and Sirt6 levels in aging mice. *Aging.* 2019;11:9348–9368. doi:10.18632/aging.102376
- Boufker HI, Lagneaux L, Fayyad-Kazan H, et al. Role of farnesoid X receptor (FXR) in the process of differentiation of bone marrow stromal cells into osteoblasts. *Bone.* 2011;49:1219–1231. doi:10.1016/j.bone.2011.08.013
- Cho SW, An JH, Park H, et al. Positive regulation of osteogenesis by bile acid through FXR. *J Bone Miner Res.* 2013;28:2109–2121. doi:10.1002/jbmr.1961
- Wu J, Ke X, Fu W, et al. Inhibition of hypoxia-induced retinal angiogenesis by specnuezhenide, an effective constituent of *Ligustrum Lucidum* Ait. through suppression of the HIF-1 α /VEGF signaling pathway. *Molecules.* 2016;21:1756. doi:10.3390/molecules21121756
- Chen B, Wang L, Li L, et al. *Fructus Ligustri Lucidi* in osteoporosis: a review of its pharmacology, phytochemistry, pharmacokinetics and safety. *Molecules.* 2017;22:1469. doi:10.3390/molecules22091469
- Hu D, Huang S, Ding Y, et al. Specnuezhenide reduces carbon tetrachloride-induced liver injury in mice through inhibition of oxidative stress and hepatocyte apoptosis. *J Pharm Pharmacol.* 2022;74:191–199. doi:10.1093/jpp/rgab164
- Li Z, Huang J, Wang F, et al. Dual targeting of bile acid receptor-1 (TGR5) and farnesoid X receptor (FXR) prevents estrogen-dependent bone loss in mice. *J Bone Miner Res.* 2019;34(4):765–776. doi:10.1002/jbmr.3652
- Ye X, Jiang J, Yang J, et al. Specnuezhenide suppresses diabetes-induced bone loss by inhibiting RANKL-induced osteoclastogenesis. *Acta Biochim Biophys Sin.* 2022;54:1080–1089. doi:10.3724/abbs.2022094
- Dell RB, Holleran S, Ramakrishnan R. Sample size determination. *ILAR J.* 2002;43(4):207–213. doi:10.1093/ilar.43.4.207
- Ma C, Zhou X, Xu K, et al. Specnuezhenide decreases interleukin-1 β -induced inflammation in rat chondrocytes and reduces joint destruction in osteoarthritic rats. *Front Pharmacol.* 2018;9:700. doi:10.3389/fphar.2018.00700
- Nair AB, Jacob S. A simple practice guide for dose conversion between animals and human. *J Basic Clin Pharm.* 2016;7:27–31. doi:10.4103/0976-0105.177703

21. Chin KY, Abdul-Majeed S, Mohamed N, et al. The effects of tocotrienol and lovastatin co-supplementation on bone dynamic histomorphometry and bone morphogenetic protein-2 expression in rats with estrogen deficiency. *Nutrients*. 2017;9:143. doi:10.3390/nu9020143
22. Ge Q, Yang S, Qian Y, et al. Ambient PM2.5 exposure and bone homeostasis: analysis of UK biobank data and experimental studies in mice and in vitro. *Environ Health Perspect*. 2023;131:107002. doi:10.1289/EHP11646
23. Hu L, Xie X, Xue H, et al. MiR-1224-5p modulates osteogenesis by coordinating osteoblast/osteoclast differentiation via the Rap1 signaling target ADCY2. *Exp Mol Med*. 2022;54:961–972. doi:10.1038/s12276-022-00799-9
24. Wang Y, Hu X, Zhang L, et al. Bioinspired extracellular vesicles embedded with black phosphorus for molecular recognition-guided biomineralization. *Nat Commun*. 2019;27:2829. doi:10.1038/s41467-019-10761-5
25. Xu J, Wang Y, Li J, et al. IL-12p40 impairs mesenchymal stem cell-mediated bone regeneration via CD4+ T cells. *Cell Death Differ*. 2016;23:1941–1951. doi:10.1038/cdd.2016.72
26. Rifai OA, Chow J, Lacombe J, et al. Proprotein convertase furin regulates osteocalcin and bone endocrine function. *J Clin Invest*. 2017;127:4104–4117. doi:10.1172/JCI93437
27. Sasao T, Fukuda Y, Yoshida S, et al. Population doubling level-dependent change of secreted glycosaminoglycan in equine bone marrow-derived mesenchymal stem cells. *J Equine Sci*. 2015;26:73–80. doi:10.1294/jes.26.73
28. Zhang J, Zhang W, Dai J, et al. Overexpression of Dlx2 enhances osteogenic differentiation of BMSCs and MC3T3-E1 cells via direct upregulation of osteocalcin and ALP. *Int J Oral Sci*. 2019;11:12. doi:10.1038/s41368-019-0046-1
29. Jeong JW, Ji SY, Lee H, et al. Fermented sea tangle (*Laminaria japonica* Aresch) suppresses RANKL-induced osteoclastogenesis by scavenging ROS in RAW 264.7 cells. *Foods*. 2019;8:290. doi:10.3390/foods8080290
30. Wang C, Gao H, Cai E, et al. Protective effects of *Acanthopanax senticosus* - *Ligustrum lucidum* combination on bone marrow suppression induced by chemotherapy in mice. *Biomed Pharmacother*. 2019;109:2062–2069. doi:10.1016/j.biopha.2018.11.071
31. Xu P, Lin B, Deng X, et al. VDR activation attenuates osteoblastic ferroptosis and senescence by stimulating the Nrf2/GPX4 pathway in age-related osteoporosis. *Free Radic Biol Med*. 2022;193:720–735. doi:10.1016/j.freeradbiomed.2022.11.013
32. El-Baz FK, Saleh DO, Abdel jaleel GA, et al. *Heamatococcus pluvialis* ameliorates bone loss in experimentally-induced osteoporosis in rats via the regulation of OPG/RANKL pathway. *Biomed Pharmacother*. 2019;116:109017. doi:10.1016/j.biopha.2019.109017
33. Yang Q, Zou Y, Wei X, et al. PTP1B knockdown alleviates BMSCs senescence via activating AMPK-mediated mitophagy and promotes osteogenesis in senile osteoporosis. *Biochim Biophys Acta Mol Basis Dis*. 2023;1869:166795. doi:10.1016/j.bbdis.2023.166795
34. Wang Q, Wang G, Wang B, et al. Activation of TGR5 promotes osteoblastic cell differentiation and mineralization. *Biomed Pharmacother*. 2018;108:1797–1803. doi:10.1016/j.biopha.2018.08.093
35. Fujimori K, Iguchi Y, Yamashita Y, et al. Synthesis of novel farnesoid X receptor agonists and validation of their efficacy in activating differentiation of mouse bone marrow-derived mesenchymal stem cells into osteoblasts. *Molecules*. 2019;24:4155. doi:10.3390/molecules24224155
36. Zhang Y, Wei J, Feng X, et al. Folic acid supplementation prevents high body fat-induced bone loss through TGR5 signaling pathways. *Food Funct*. 2024;15:4193–4206. doi:10.1039/D4FO00404C
37. Liu M, Jin F, Zhang S, et al. Activation of farnesoid X receptor signaling by geniposidic acid promotes osteogenesis. *Phytomedicine*. 2022;103:154258. doi:10.1016/j.phymed.2022.154258

Drug Design, Development and Therapy

Publish your work in this journal

Drug Design, Development and Therapy is an international, peer-reviewed open-access journal that spans the spectrum of drug design and development through to clinical applications. Clinical outcomes, patient safety, and programs for the development and effective, safe, and sustained use of medicines are a feature of the journal, which has also been accepted for indexing on PubMed Central. The manuscript management system is completely online and includes a very quick and fair peer-review system, which is all easy to use. Visit <http://www.dovepress.com/testimonials.php> to read real quotes from published authors.

Submit your manuscript here: <https://www.dovepress.com/drug-design-development-and-therapy-journal>

Dovepress
Taylor & Francis Group